Improvements in Axle Box Acceleration Measurements for the Detection of Light Squats in Railway Infrastructure

Zili Li, Maria Molodova, Alfredo Núñez, *Senior Member, IEEE*, and Rolf Dollevoet

***Abstract*—Squats are a type of short-wave rolling contact fatigue defect whose early detection can contribute to cost reductions in the railway industry. This paper demonstrates how the early detection of squats is possible via enhanced instrumentation based on axle box acceleration (ABA) and adequate postprocessing. Three improvements are discussed. The first corresponds to the use of longitudinal ABA to enhance measurement sensitivity to light squats. Compared to vertical ABA, longitudinal ABA does not contain the vibrations of the rail, fastening, sleepers, and ballast, and thus, the impact-related vibration is considerably stronger in the signal. The second improvement considers the use of multiple sensors, noise-reduction techniques, and repeated measurements. Due to hunting, the wheels of a measuring train do not always pass over small squats; thus, light squats are more likely to be detected using multiple sensors and multiple measurement runs. The third improvement concerns the signal-processing solution for the reduction of disturbances from wheel defects. Extensive field measurements show that these improvements make the characteristics of squats more visible in signals and allow the squats to be distinguished from vibrations of other origins.**

***Index Terms*—Axle box acceleration (ABA), rail transportation maintenance, railway monitoring, surface defects on railway rails.**

I. Introduction

DIFFERENT condition-monitoring systems have been developed recently in the railway industry to ease the process of manual inspection [1]–[5]. Currently, the most widely used method for monitoring railway tracks is ultrasonic testing [6]. However, this method, only reliably detects severe defects with cracks deeper than 5 mm. Other methods, such as visual inspection [7], alternating current field [8], image recognition [9], strain gage instrumented wheel [10], acoustic detection [11], and guided-wave-based health monitoring [12], have been proposed, each of which has different advantages in terms of cost, reliability, and robustness. This paper focuses on the use of axle box acceleration (ABA) measurements. In previous studies, accelerometers have been used for modeling, monitoring, and control in different systems (see, for example, [13]–[16]). In the case of railway track monitoring, this type of sensor has succeeded in the detection of severe corrugation, welds, and poor-quality insulated joints [17]–[19]. The main advantages of the ABA compared to other railway condition-monitoring systems are its lower cost, ease of maintenance, and implementation in trains running at commercial speeds. In Dutch railways, vertical ABA was employed to detect defects, such as severe corrugation and poor-quality welds. In other countries, such as Japan [19], Poland [20], Italy [21], and Korea [17], ABA systems have also been implemented for the analysis of railway track defects. For a better understanding of the state-of-the-art use of ABA for monitoring railway infrastructure, a summary of past research is provided in Table I.

TABLE I
Reported Implementations of ABA Systems

ABA implementation	*Defects studied*	*Frequency range*	*Railway network*
Vertical ABA, 2 sensors, 80 km/h	Corrugation, wavelengths 0.055 – 0.080 m	Measured up to 2864 Hz	Polish State Railways Network [20]
Vertical ABA Lateral ABA	Corrugation Lateral discontinuity, curve rail wear, damaged switches	Analysis between 25 Hz and 1246 Hz	Subway of Milan, Italy [21],[22]
Vertical ABA Lateral ABA	Alignment, zones of large lateral force, track irregularities below 100 Hz	Analysis up to 100 Hz	Japanese high-speed railways [23]
Vertical ABA Lateral ABA speed 300 km/h	Long wavelength irregularities, from 3 m to 200 m, both lateral and vertical irregularities	Analysis up to 2,048 Hz	Korean Train Express, high-speed line [17]

This paper addresses the use of ABA for the detection of squats, which are a major type of short-wave rolling contact fatigue. Squats may cause rail fracture and catastrophic consequences if not treated in time. Previous studies on the use of ABA for the detection of squats have revealed that the existing ABA instrumentation and signal processing must be improved to increase the hit rate of detection for light squats; this paper discusses such improvements. The first improvement considers the use of longitudinal ABA to enhance measurement

Manuscript received April 25, 2014; revised April 28, 2014, July 17, 2014, and November 28, 2014; accepted November 29, 2014. Date of publication January 9, 2015; date of current version May 15, 2015. This work was supported in part by the Dutch railway infrastructure manager ProRail and in part by the Dutch Technology Foundation STW, which is part of the Netherlands Organization for Scientific Research (NWO) and is partly funded by the Ministry of Economic Affairs.

The authors are with the Section of Road and Railway Engineering, Delft University of Technology, 2628 Delft, The Netherlands (e-mail: Z.Li@tudelft.nl; M.Molodova@tudelft.nl; A. A.NunezVicencio@tudelft.nl; R.P.B.J.Dollevoet@tudelft.nl).

Color versions of one or more of the figures in this paper are available online at http://ieeexplore.ieee.org.

Digital Object Identifier 10.1109/TIE.2015.2389761

sensitivity to light squats [24]. In the analysis of railway wheel vibrations using the hammer test, the frequency contents of the transfer function obtained in the longitudinal direction are stronger than in the vertical direction between 820 and 2200 Hz. Hence, the frequency contents above 1000 Hz of ABA are stronger in the longitudinal ABA signal for light squats, which is consistent with a previous report [25] that frequencies up to 2000 Hz are related to squats. The second improvement considers noise-reduction techniques for the multiple signals coming from different ABA sensors and repeated measurements. Multiple sensors and repeated measurements are used to reduce the effects of hunting, which reduces the hit rate for the detection of smaller defects when the wheels do not pass over them. Finally, we address a typical practical problem induced by wheel defects. In practice, wheel defects have a repetitive pattern; thus, this paper discusses how noise-reduction methods can be used to reduce their effect on ABA signals.

Extensive field tests of different Dutch tracks have shown that these improvements made the characteristics of squats more visible in ABA signals. The improvements discussed in this paper are the basis of an enhanced ABA prototype. A detection method based on wavelets was previously proposed using this prototype; however, the fundamentals behind the implementation of this prototype have not yet been discussed. The improvements discussed in this paper allowed for the implementation of more efficient detection algorithms and forecast models for defects, which are essential components of any health-monitoring and fault detection system for the different components of the railway infrastructure [24]–[32].

II. Monitoring Framework for Railway Infrastructure Using ABA Measurements

The proper frequency content of an ABA measurement can be used to improve the detection of light and moderate squats. Several techniques are available to investigate the frequency content of signals, but not all of these techniques provide accurate information. Wavelet analysis is used in this paper because the time and frequency resolutions are high. Wavelet analysis has already been reported as an appropriate method for the investigation of nonstationary phenomena with local changes in the frequency components, such as structural damage detection and crack identification [22], [33]. To formalize the monitoring tasks of railway network infrastructure, we represent the condition of the track at an interval time T and location x with the nonparametric response function $H_{T,x}(f)$, which is given by the wavelet power spectrum (WPS) in the frequency domain f. The railway track system is shown in Fig. 1.

When the track is in healthy conditions, the function will present local maxima and minima corresponding mainly to the natural responses of the track. Those natural responses differ for each track, different type of sleeper, and between slab and ballasted tracks. We define the healthy response of a track as $H_{T,R}(f)$, which is valid for tracks with similar structural characteristics. When the function $H_{T,x}(f)$ at a certain location x differs significantly from the defined healthy response $H_{T,R}(f)$, the frequencies that concentrate most of the energy will provide information about the type of irregularity around

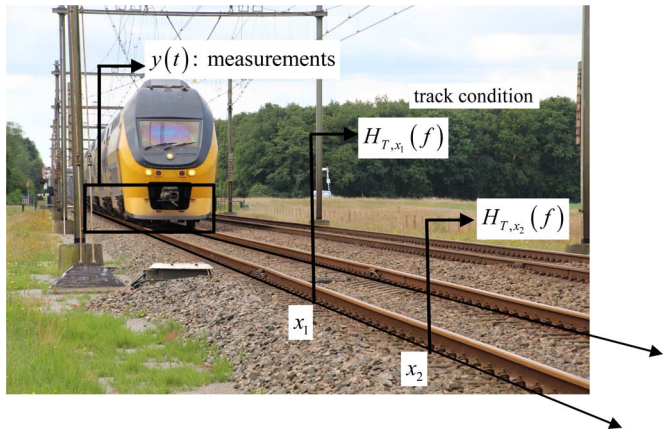

Fig. 1. Track conditions are assessed via signal-processing methods using onboard measurements.

location x at time t. To estimate $H_{T,x}(f)$, a set of onboard measurements $y(t)$ are available at $t \in T$: the position of the train $x(t)$ (given by a GPS), the velocity of the train $v(t)$, and a set of ABA measurements $a(t)$ in the vertical and longitudinal directions collected in different bogies.

This paper considers two responses: longitudinal ABA, i.e., $H^{\mathrm{L}}_{T,x}(f)$, and vertical ABA, i.e., $H^{\mathrm{V}}_{T,x}(f)$. To calculate both responses from the measurements, the wavelet coefficients are defined as follows [34]:

$$H_{T,x}(f) = \left|W_n^2(s)\right| \tag{1}$$

$$W_n(s) = \sum_{n'=0}^{N-1} x_{n'} \psi^* \left(\frac{(n'-n)\delta_t}{s} \right) \tag{2}$$

where x_n is a time series with a time step of δ_t, n is the time index, $n' = 0, \ldots, N-1$ is the time shift operator, ψ is a mother wavelet, which is a locally limited function, ψ^* is a family of wavelets deduced from the mother wavelet by different translations and scaling, * indicates a complex conjugate, s is a wavelet scale, $s > 0$, and $W_n(s)$ are wavelet coefficients. In this paper, the Morlet function is used as a mother wavelet. The wavelet scale is related to the Fourier period (or inverse frequency). The wavelet transform can also be considered as a linear filtering operation that involves a set of parallel filters. The plot of the frequency response $H_{T,x}(f)$ for an interval of consecutive positions $x \in \mathrm{X}$ is termed a scalogram. A vertical slice of a scalogram for a given distance x is the function $H_{T,x}(f)$, which provides a measure of the local spectrum. For simplicity, we directly discuss the scalograms in this paper. The next section analyzes the design methodology and the use of longitudinal ABA in particular.

III. Design Methodology Including Longitudinal ABA Measurements

A. Use of Longitudinal ABA Measurements

The purpose of using longitudinal ABA is to detect light squats/indentations whose lengths are typically 10–30 mm. For a normal traffic speed of 140 km/h (or 39 m/s) and for the speed of the measuring train (100–110 km/h), light squats cause

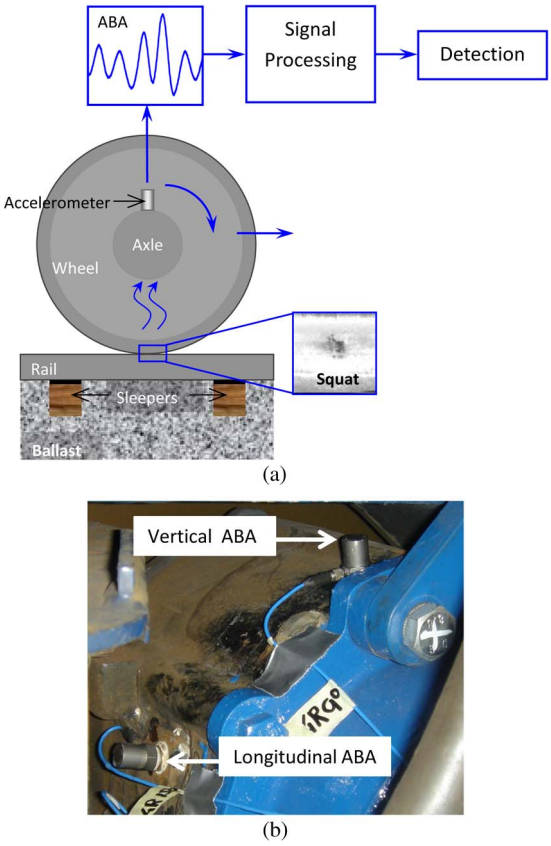

Fig. 2. (a) Schematic of the new instrumentation setup for ABA measurements. (b) Implemented prototype.

frequency contents of 1–4 kHz for the forced vibration/impact part. The instrumentation setup for ABA measurements is shown in Fig. 2.

When a wheel runs over a squat, the vibrations due to the impact are excited and transferred to the wheel axle. The frequency contents related to squats can be extracted from the ABA measurements, and a decision is made regarding the presence of a defect and its severity. We used general-purpose uniaxial piezoelectric accelerometers in the implementation. The dynamic range of the accelerometer was above the maximum ABA magnitude of 700 m/s^2. The sampling frequency of the ABA measurements was 25.6 kHz. As our interest is frequencies up to 2.5 kHz, this sampling frequency is sufficient for accurate measurements. GPS coordinates were measured with a sampling frequency of 1 Hz, synchronized with the ABA and interpolated to 25.6 kHz. ABA was installed on the nondriven axle to reduce noise coupling from the drive system.

Different track components affect the ABA measurements in different ways. For a more theoretical background, including deduction of the wheelset–track system transfer function, [13] is suggested. In Fig. 3, a short-wave defect causes an impact-like wheel–rail interaction. As the purpose is to detect impact-related events, signal components that are not characteristic of impact are considered noise. The resulting vibrations measured in vertical ABA include those of the bearing, wheelset, rail, railpad and fastening, sleeper, ballast and subgrade. In contrast, in longitudinal ABA, the vibration only includes those of the bearing and wheelset. Due to axial symmetry, the vibrations

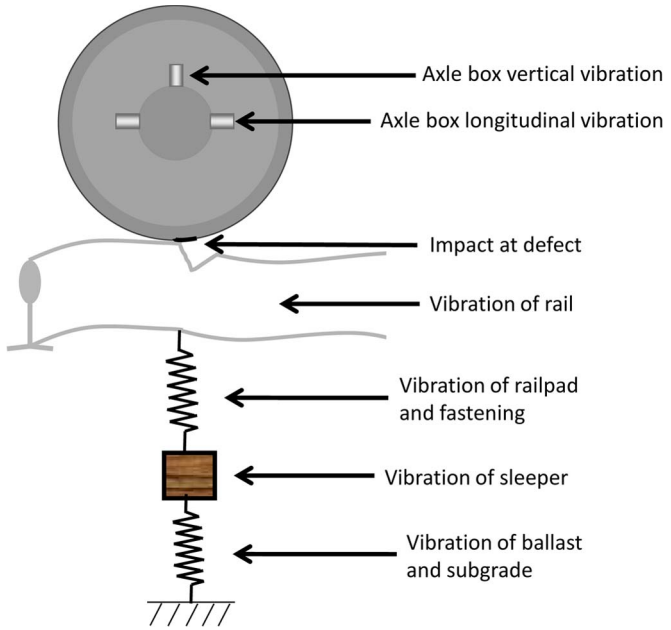

Fig. 3. Measured vibrations of an impact-like wheel–rail interaction.

of the bearing and wheelset contained in the longitudinal ABA should be nearly the same as in the vertical ABA. Many of the vibrations of the rail, railpad and fastening, sleeper, ballast, and subgrade are also excited by normal wheel–rail rolling contact and are thus not characteristic of short-wave defects (noise for the detection of squats). For example, the noise from elastic deformation of the subgrade is in the low-frequency range and thus does not affect detection [25], [26]. However, many of the high-frequency vibration modes of the wheelset can only be substantially excited by impact-like wheel–rail contact. Therefore, longitudinal ABA contains less noise and is more sensitive to light squats/indentation defects.

B. Theoretical and Practical Analysis of Vibration Modes of the Wheel

One method to prove the concept that longitudinal ABA has a higher signal-to-noise ratio at squats than vertical ABA is by performing hammer tests on the wheel and investigating the transfer function between the load applied at the wheel rim and the response measured at the axle box. In this manner, the transmission of vibrations from the wheel–rail interface to the axle can be analyzed. For a better understanding of the vibrational modes of the wheel, consider Fig. 4, in which the lateral, vertical, and longitudinal directions are denoted by z, y, and x, respectively.

Theoretically, the vibrational modes of a wheel can be obtained by stress-free FE modal analysis, considering a single wheel and half of the axle. The wheel modes of interest and their classification are shown in Fig. 4, where the red and blue colors indicate the maximum amplitudes of the vibrations in opposite directions of the axle. The theoretical resonant modes of the wheel are symmetrical or antisymmetrical in the $x-y$ plane about the axle at which accelerations are measured.

The hammer test is an impact test conducted on the wheel in which the impact load and accelerations on the axle of

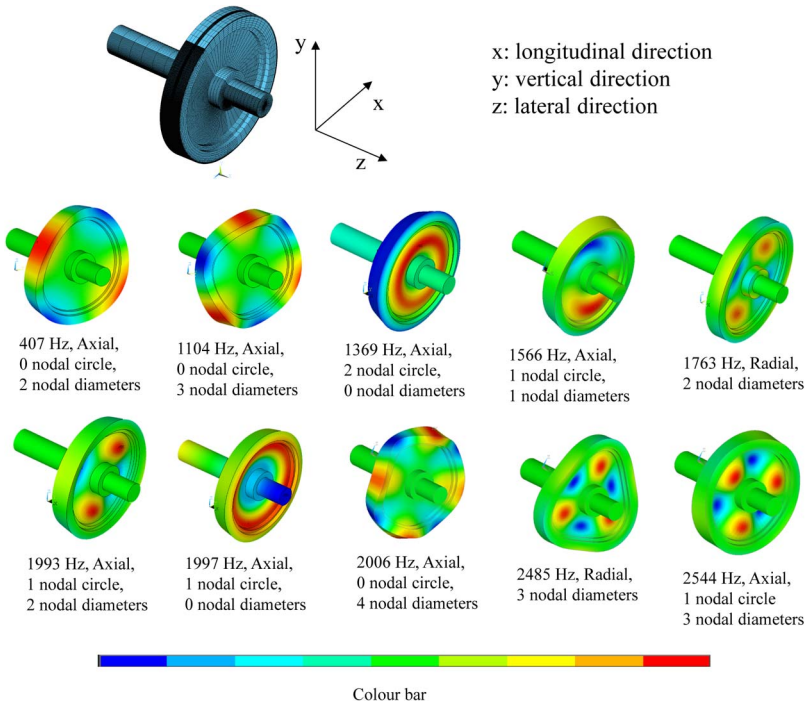

Fig. 4. Finite-element (FE) model of the wheel and wheel mode shapes; colors indicate displacement along the axis directions.

the wheel are measured to calculate the frequency response function. The impact load applied with a hammer was measured with a force sensor in the hammer. The response of the wheel was measured with accelerometers mounted on the axle on the vertical and longitudinal directions. The load was applied to the wheel rim in the vertical direction. Fig. 5 shows that the transfer function obtained in the longitudinal direction is stronger than that in the vertical direction between 820 and 2200 Hz. Hence, the frequency contents in this range in the case of light squats should be stronger in longitudinal ABA. The transfer function shown in Fig. 5(b) is called inertance, which is, by definition, acceleration $[\mathrm{m/s^2}]$ divided by force [N], where the unit $[\mathrm{m/N \cdot s^2}]$ is equivalent to [1/kg]. A standard procedure using hammer tests was conducted to obtain the inertance [35]. First, the wheel was excited five times with the hammer, and the average force $F(t)$ and average acceleration from the sensors $a(t)$ were calculated to reduce random error. Then, the measured signals were transformed into the frequency domain by fast Fourier transform, and the inertance function $I(j\omega)$ was calculated as follows:

$$I(j\omega) = \frac{S_{\mathrm{aF}}(j\omega)}{S_{\mathrm{FF}}(j\omega)} = \frac{\sum_{n=1}^{N}\sum_{m=1}^{N-m-1} a[m+n]F[m]e^{-j\omega n}}{\sum_{n=1}^{N}\sum_{m=1}^{N-m-1} F[m+n]F[m]e^{-j\omega n}} \tag{3}$$

where S_{aF} is the cross spectrum between force and acceleration, S_{FF} is the autospectrum of the force, N is the number of data points sampled, and $\omega = 2\pi f$, with f being the frequencies in hertz. The frequency range of the inertance function is defined by the hammers used and the applicability of the measured data, which, in this case, cover frequencies between 50 and 3000 Hz.

In the case of longitudinal and vertical accelerations (x- and y-directions, respectively), axial symmetry of the wheel permits some correlation with squats (in the plane of the wheel). In fact, in the region of interest between 400 and 2000 Hz, we can observe a correspondence between many of the peaks and dips of both vertical and longitudinal signals in Fig. 5(b), meaning that there are many excited modes in common. In normal operating conditions, the wheel is loaded in the vertical direction, resulting in a higher vibration magnitude than in the case in which the wheel is lifted up for the hammer test. However, during the hammer test measurements in Fig. 5(a), the wheel was lifted (at the bogie frame), and thus, the wheel load was only the weight of the wheelset, which is considerably less than the typical load of the train. Hence, the system was "theoretically" under the investigated unloaded condition with no noise from the vibrations of the track components, and longitudinal ABA has higher sensitivity to the impact of the hammer in the high-frequency range. In theory, the sensitivity of vertical and longitudinal ABA should be equal due to axial symmetry. The lower sensitivity of vertical ABA can be attributed to the fact that the wheelset hung on the bogie frame through the first suspension, which included damping from the damper and rubber pads. Under normal loading conditions, this concept was later proven in the field with extensive measurements. In this sense, the loading of the wheel is not the most influential factor; thus, the mounting position of the vertical sensor on the highest loading path of the wheel or less-loaded location should not significantly change the resulting signal. Fig. 5(b) shows that the longitudinal response is between one and ten times the vertical response in the frequency range of interest, i.e., 1000–2500 Hz, depending on the modes of the wheel. In longitudinal ABA, the response is theoretically purely due to an impact; thus, the sensitivity can be defined as 100%. However,

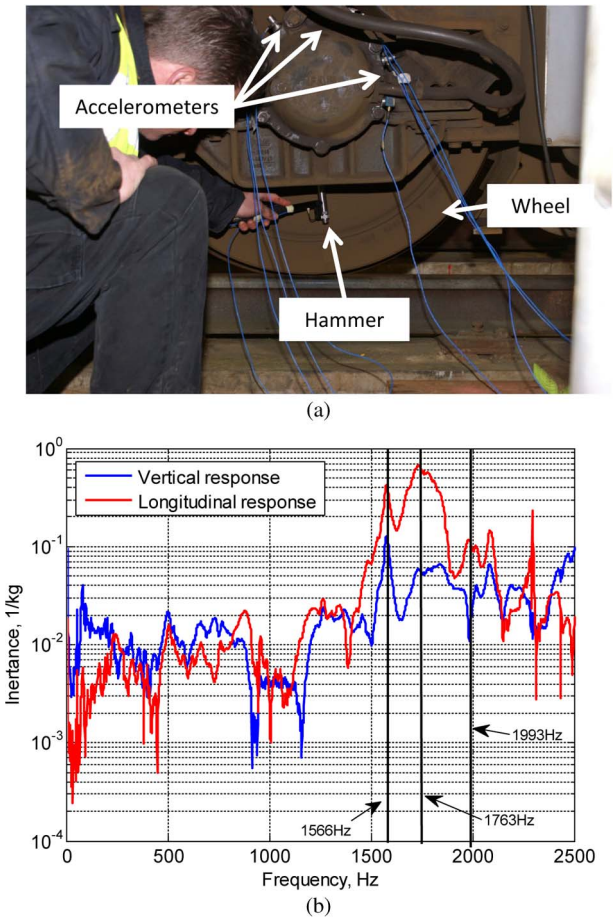

Fig. 5. (a) Hammer test on the wheel, from which (b) inertance is calculated.

in vertical ABA, the response to an impact consists of the wheel vibration and the remainder excited by loading, and other components are considered as noise.

Finally, in practice, for many ABA measurements since 2009, the magnitude of longitudinal ABA at light squats/indentation is higher than that of vertical ABA. For example, in Fig. 6, at the same light defect, the magnitude of longitudinal ABA is 1.4 times higher than that of vertical ABA. A particularly important effect also occurs with the frequency contents. As shown in Fig. 6, the WPS is considerably stronger for the longitudinal ABA measurement. Due to this effect on the power spectrum, the use of longitudinal ABA is significant for improving the detection of light squats. In the case of moderate and severe squats, whose related frequency contents are different from those of light squats, the use of longitudinal ABA increased the hit rate from 60% to 100% [26].

C. Additional Analysis and Remarks

Regarding the sensitivity of lateral ABA to squats, theoretically, it is not evident how the vibrations caused by the impact at squats can be transmitted from the wheel–rail interface to the axle in the lateral direction. A squat causes an impact to a wheel in the vertical direction, which induces forced vibration of the wheelset. The mode shapes of the wheelset can be classified into two groups: wheel modes and axle modes. According to [36] and [37], all wheel vibration modes are symmetric or antisymmetric with respect to the axle. Thus, squat-induced wheel vibration can be measured in both the vertical and longitudinal directions on the axle box. According to [37], the axle modes can be classified into three groups: flexural, torsional, and compressional. Flexural modes are excited by vertical impacts and have components in the x- and y-directions, whereas this component will be small or zero in the z-direction. Torsional modes are nonsymmetric with respect to the wheel and axle and have no components in the z-direction. Compressional modes are indeed mainly in the lateral (z) direction but have no components in the longitudinal or vertical directions; thus, the likelihood of excitation by a vertical force is small. Therefore, in summary, the vibration modes excited by a vertical force are mainly in the vertical $(x-y)$ plane; thus, the sensitivity for lateral acceleration to measure squats is lower than that of longitudinal ABA.

In our approach, to keep the concept flexible, we do not propose an optimal mounting position for the sensor because there are different axle box structures in different rolling stocks. On some axle boxes, it might not even be possible to mount the sensors in certain locations; in those cases, the use of triaxial sensors at possible locations to measure both vertical and longitudinal ABA would be suggested. Different arrangements can give rise to different sensitivity of squats.

Regarding the coupling effects between the axle box and piezoelectric elements, according to [38], different mounting techniques of accelerometers such as cementing stud, wax, or magnet will influence the frequency response only in the frequency range above 5 kHz, which is out of our frequency range of interest. In the next section, noise reduction is discussed for improvement of the signal-to-noise ratio.

IV. Noise Reduction in ABA Signals

To distinguish a small defect from noise, noise-reduction techniques must be applied. Rompelman and Ros [39] presented a noise-reduction technique based on coherent averaging. The coherent averaging method is based on the principle that the time signal measured immediately after applying a stimulus contains an invariant response to the stimulus and a noise component. When averaging a number of similar time signals, all invariant responses are systematically added, whereas the random noise components are summed and tend toward zero. Noise reduction becomes more effective when the number of averaged samples increases.

For the application of an averaging technique, the exact moment of each stimulus must be known. In the case of ABA measurements, repeated signals were recorded on the same track section and overlapped such that the responses at certain short track defects began at the same location. To overlap the signals, the cross correlation of the signals was calculated. The cross-correlation function is a measure of the similarity between two data sets and is often applied to determine the time shift that maximizes the similarity of two data sets. One data set is moved relative to the other, the corresponding values of the two data sets are multiplied together, and the products

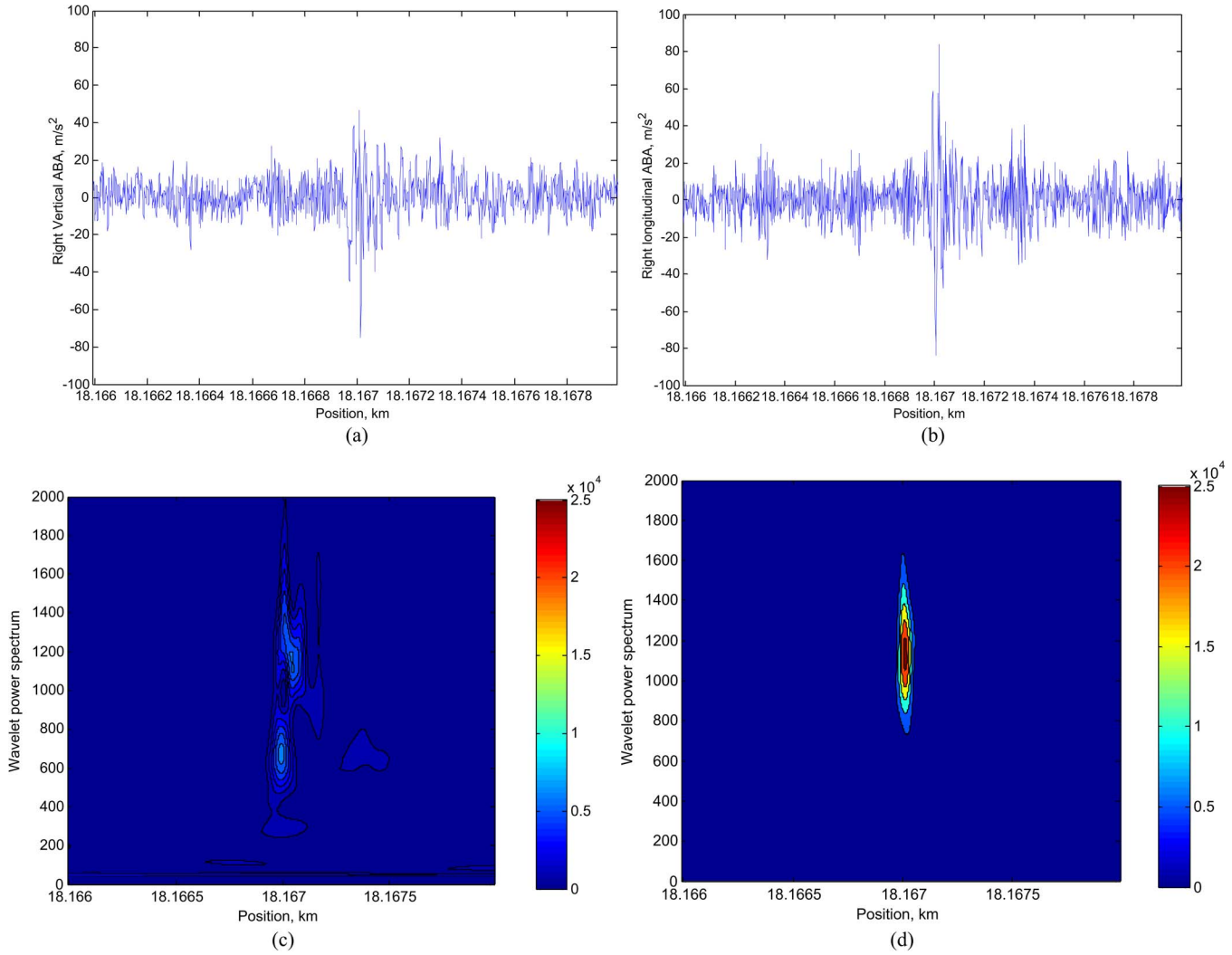

Fig. 6. ABA measurements at a light squat using the prototype. The defect is located at approximately 18.167 km. (a) Vertical ABA measurement. (b) Longitudinal ABA measurement. (c) WPS of vertical ABA. (d) WPS of longitudinal ABA.

are summed to give the value of cross correlation. The cross correlation of two data sets x_t and y_t is expressed as follows:

$$\varphi(\tau) = \sum_k x_k y_{k+\tau} \tag{4}$$

where $\varphi(\tau)$ is the cross correlation, and τ is the displacement of data set y_t relative to data set x_t. When two data sets are nearly the same, the product is typically positive, and the cross correlation is large. Two data sets might be dissimilar when lined up in one way but might be similar when one set is properly shifted with respect to the other; thus, the cross correlation is a function of the relative shift between the sets.

To study the effect of averaging on noise reduction and, thus, the detection of squats, a single measurement was compared to the averages of three and six signals. In the example below, the vertical ABA responses at four small rail surface defects were investigated. The defects are shown in Fig. 7(a), one of which (T1L) was located at a thermite weld. These defects appear with periodicity of approximately 3 m; hence, they should have originated from a hard object indented into the wheel. These defects are studied because they may become a source of squat initiation. However, the defects are extremely small, and their detection is more difficult than the detection of mature squats. To analyze the ABA signals, scalograms obtained based on the WPS are considered [6], [40], [41]. In this paper, scalograms are used to define the time–frequency relationship of squats with the ABA signal. Fig. 7(b)–(d) presents scalograms of vertical ABA measurements around the defects presented in Fig. 7(a), with an indication of defect locations.

The red color represents a high signal energy level due to the impact at a defect. In the scalogram of a single measurement [see Fig. 7(b)], the responses at defects K and T1L have clear frequency characteristics between 1000 and 2000 Hz. The red area at the frequencies below 600 Hz at 8.8 m corresponds to the thermite weld. The responses at defects J and L cannot be easily distinguished from the noise. In the scalogram of the average of three signals, the responses at J and L become more pronounced [see Fig. 7(c)]. The frequency characteristics at these defects are between 500 and 1500 Hz. Although there is less noise in this signal, there are still some locations that can be considered as a defect, such as, for example, at approximately

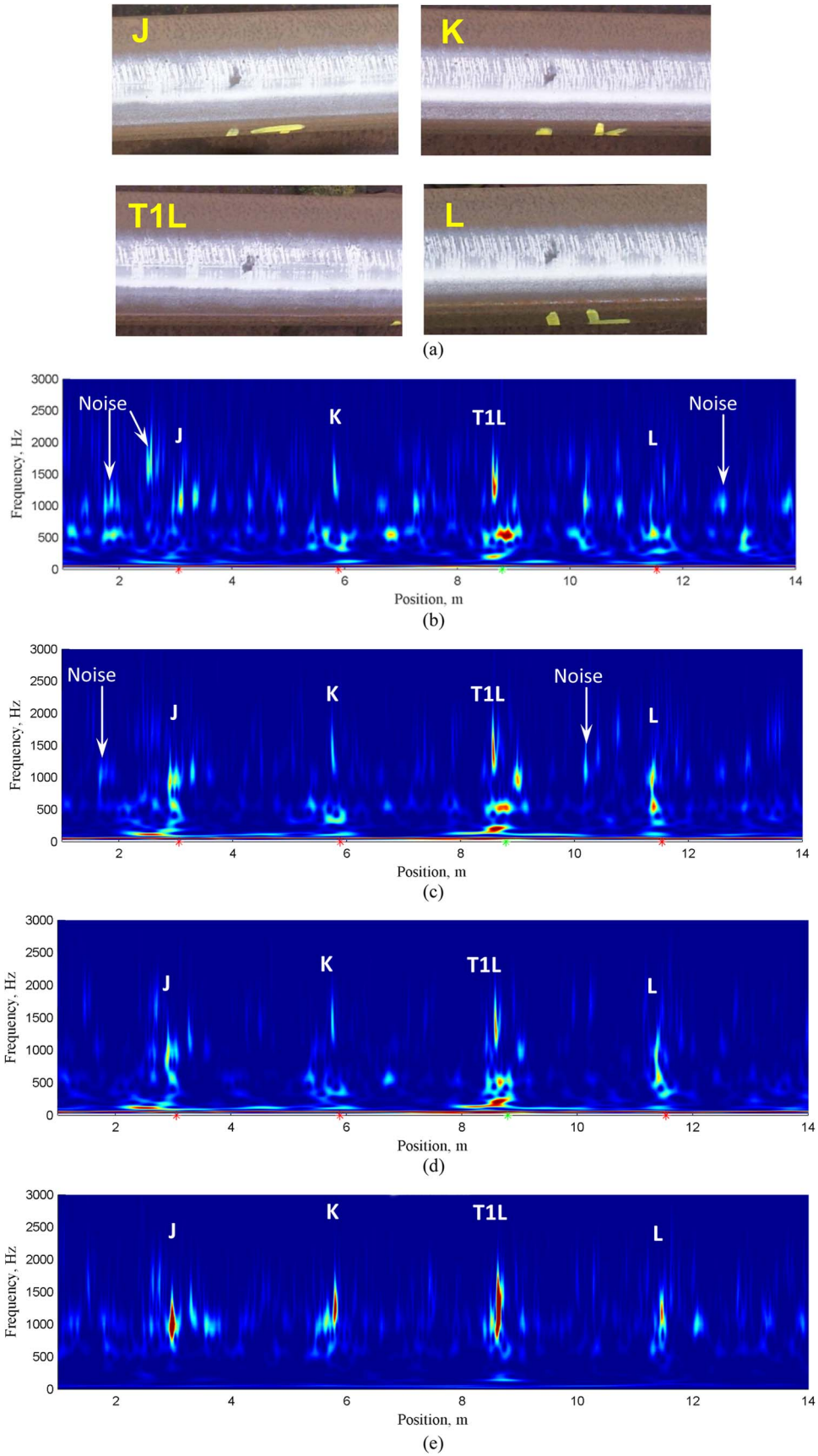

Fig. 7. Scalograms of defects in (a) using (b) one, (c) three, and (d) six ABA vertical signals and (e) a scalogram of six averaged longitudinal ABA signals. (a) Detected rail surface defects (trivial defects). (b) Single ABA vertical measurement. (c) Averaging of three ABA vertical measurements. (d) Averaging of six ABA vertical measurements. (e) Averaging of six ABA longitudinal measurements.

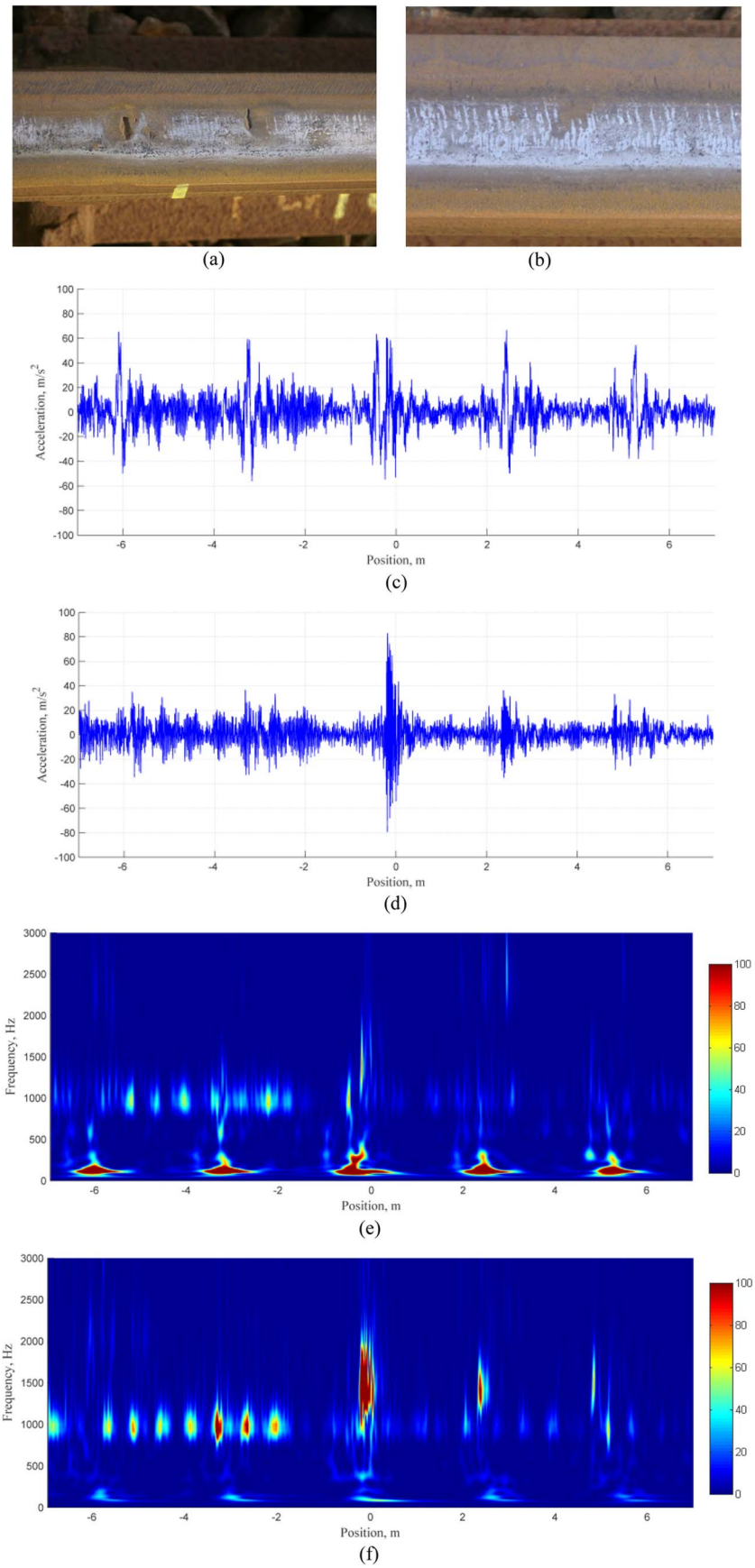

Fig. 8. (a) Severe squat after grinding at position 0 m and (b) light squat at position 5 m. (c) Vertical and (d) longitudinal ABA around two squats, at positions 0 and 5 m, with repetitive peaks excited by a wheel defect. Scalograms of (e) vertical ABA and (f) longitudinal ABA around two squats, at 0 and 5 m, with repetitive peaks excited by a wheel defect.

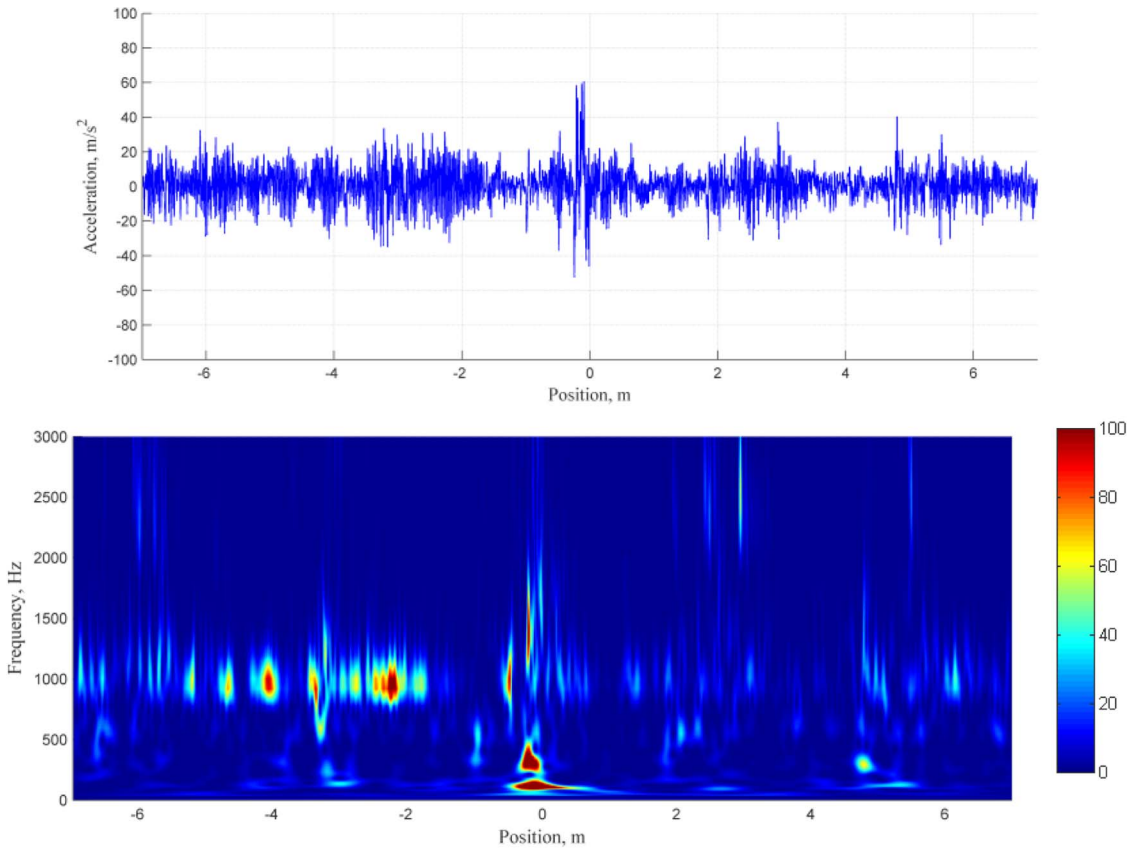

Fig. 9. Vertical ABA and its scalogram after filtering out repetitive peaks excited by a wheel defect.

1.8 and 10.2 m. In the scalogram of the average of six signals, the correspondence between defects and the ABA response becomes evident [see Fig. 7(d)]. The scalogram in Fig. 7(e) demonstrates the effect of using longitudinal ABA. Fig. 7(e) shows the average of six longitudinal signals. The frequency characteristics at defects in longitudinal ABA are between 600 and 2000 Hz. The signals below 600 Hz are clean (no red areas are observed). Above 600 Hz, the response is stronger than for vertical ABA in Fig. 7(d), as expected from the hammer test on the wheel.

The sources of noise are different, with one of the most important related to the swing caused by bogie hunting. To reduce its effect, the use of multiple measurements and repetitive signal measurements increase hit probability. In this manner, the miss hits generated when the wheel does not run completely over the light squat are minimized. However, if the squat is not in the middle of the rolling band, the hit likelihood is low, and the likelihood to grow is also reduced. In the next section, the influence of wheel defects on ABA measurements is discussed. This problem is quite recurrent in actual measuring systems, and thus, its automatic solution is important to recognize as noise so that relevant signal components can be identified.

V. Reduction of Wheel Defects on ABA

When a wheel is damaged, the measured ABA is affected. From practical experience, optimal measurements can be obtained only after wheel reprofiling. Nevertheless, if the wheel is damaged, the signals can still be used after some signal processing.

Fig. 8 shows an example of ABA measured on wheel defects. The signals have repetitive peaks, appearing at approximately every 3 m. This signal was measured around two rail defects [see Fig. 8(a) and (b)]; the larger signal was located at abscissa 0 m, and the smaller one was located at abscissa 5 m. The peaks excited by the squats cannot be distinguished from the peaks excited by the wheel defect in Fig. 8(c). However, longitudinal ABA is less sensitive to wheel damage [see Fig. 8(d)], and the ABA response to the larger squat can easily be observed in the signal. There are also some repetitive peaks related to wheel damage in the longitudinal signal, but their magnitudes are smaller than the peaks in vertical ABA. Thus, longitudinal ABA is less affected by wheel damage, and signals measured on the damaged wheel can still be used for squat detection. To understand this result, we consider that wheel defects are often larger than squats and have different sizes and depths.

The typical length of a light squat or indentation is 10–30 mm. For a normal traffic speed of 140 km/h and for the speed of the measuring train (100–110 km/h), frequency contents of 1–4 kHz result for the forced vibration/impact part. However, a wheel flat is often longer, shallower, and more obtuse (with no "sharp" edge) than indentations/light squats, causing lower frequency vibrations. In other words, light squats cause higher frequency vibrations because their effects on the signals are more like an "ideal" impact, which, in its perfect form, has zero time duration.

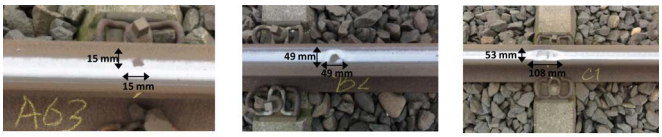

Fig. 10. Representative squat defects. (a) Light squat. (b) Moderate squat. (c) Severe squat.

Fig. 8(e) and (f) shows scalograms of the vertical and longitudinal signals. For vertical ABA, the repetitive red areas at frequencies below 250 Hz correspond to wheel damage. At 0 m, there are also frequencies with increased energy from 1000 to 2000 Hz that correspond to the squat, but this response is weak compared to the response to wheel damage. In contrast, in the scalograms of longitudinal ABA [see Fig. 8(f)], the repetitive response at frequencies below 250 Hz corresponding to wheel damage is weak, and the responses to squats at position 0 m is strong. The smaller defect is also indicated in the longitudinal signal at position 5 m by frequencies between 1000 and 2000 Hz. The other red areas in this plot, between −7 and −2 and 2 m, are related to other defects in the track. The response related to wheel defects can be excluded from the vertical signals by either filtering the ABA signal in the frequency domain by a stopband filter or by subtracting the specific repetitive pattern from ABA in the time domain. These procedures do not affect the detection of rail defects because the frequencies related to squats are in different frequency bands than those related to wheel defects.

Fig. 9(a) demonstrates the vertical ABA after removing the repetitive pattern from the time-domain signal. The peak related to the squat at position 0 m becomes clear. In the scalogram of this signal [see Fig. 9(b)], the response related to the squat at position 0 m is completely preserved even below 250 Hz, and the small defect at 5 m can also be observed in the signal. Severe wheel defects may cause strong noise in the ABA measurement. Those cases are not considered in this paper, as such defects are extremely damaging to the infrastructure and are avoided by regular inspection and maintenance of the wheels.

VI. Improved ABA Signals for Light, Moderate, and Severe Squats

Here, from a large set of validated ABA measurements at light, moderate, and severe squats, one representative case for each class of squat is presented for discussion. Pictures of the defects are shown in Fig. 10.

Moderate and severe squats can be recognized in Fig. 10 by the following characteristics: localized depression of the contact surface of the rail head with a dark spot, widening of the running band, and a shape of two lungs and cracks that start to develop [see Fig. 10(b)] or are mature [see Fig. 10(c)]. The light stage of squats may not bear some of these characteristics, but light squats can be recognized by a dark spot on the surface [see Fig. 10(a)].

As shown in Figs. 11–13, for light, moderate, and severe squats, respectively, the signals considered are the ABA measurements of two wheels of the same axle (left and right); thus,

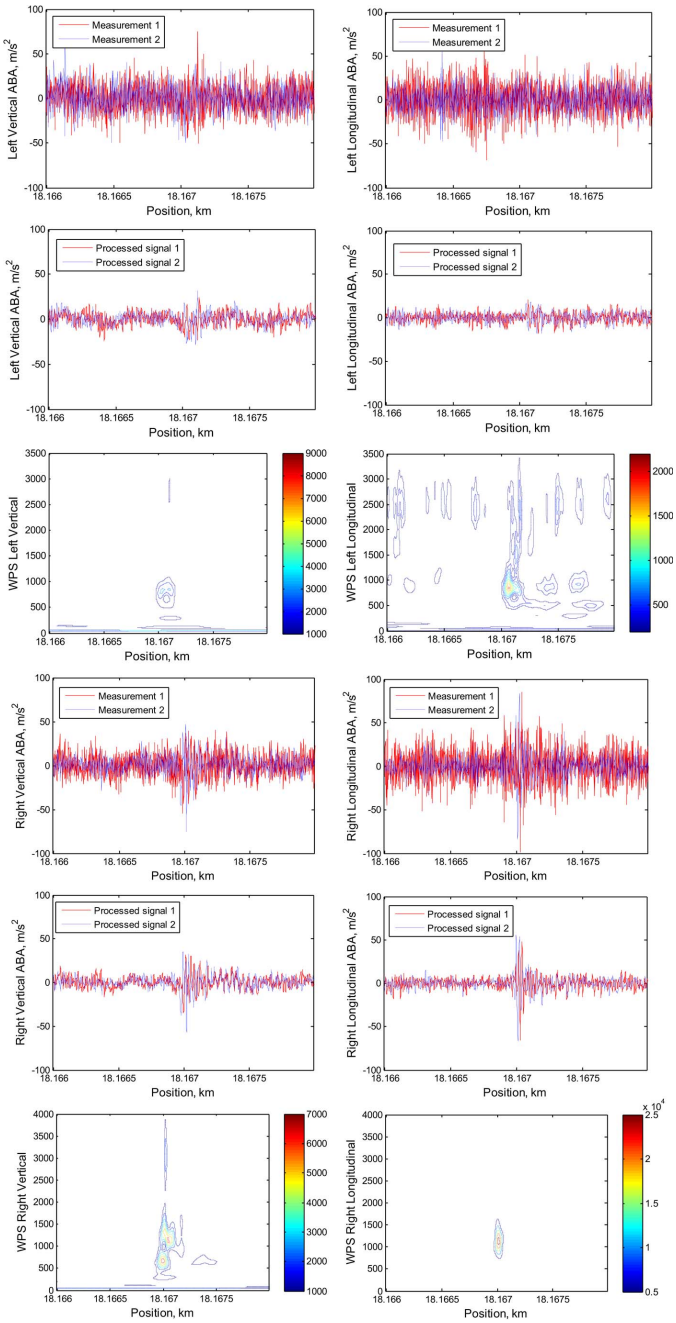

Fig. 11. Light squat responses.

squat detection on both rails is possible. However, as shown in Figs. 12 and 13, a severe squat on the "left" rail often can also be observed in the signal of the "right" rail and vice versa. This effect can increase the false alarm rate in a detection system. For this reason, the strength of the signals on the two axle ends should be compared separately to determine which rail (left or right) is infected by a squat. Future work will seek to develop intelligent algorithms to determine which rail (right or left) has the defect. In practice, however, it is more important to obtain a set of interesting locations to be evaluated by experts, who can make the decision to grind or just replace the piece of rail when many squats are found consecutively.

In Figs. 11–13, only two measurements are shown: two processed signals and the WPS corresponding to the averaged

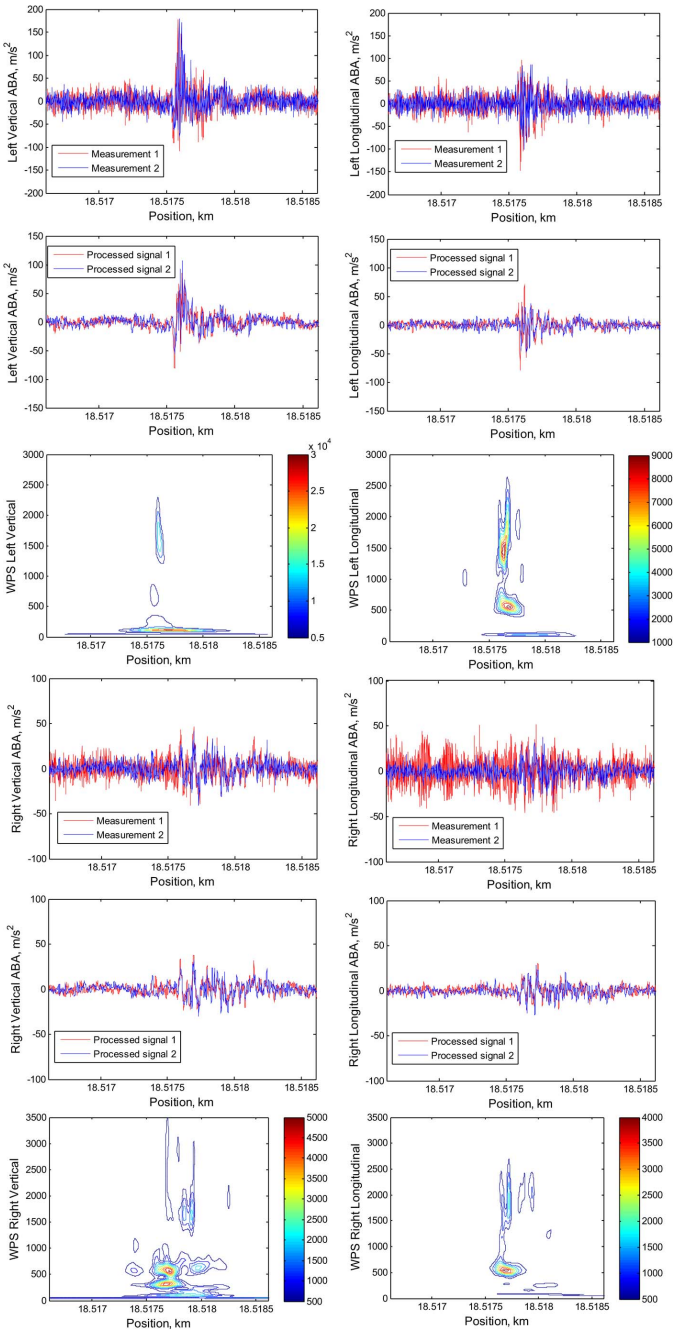

Fig. 12. Moderate squat responses.

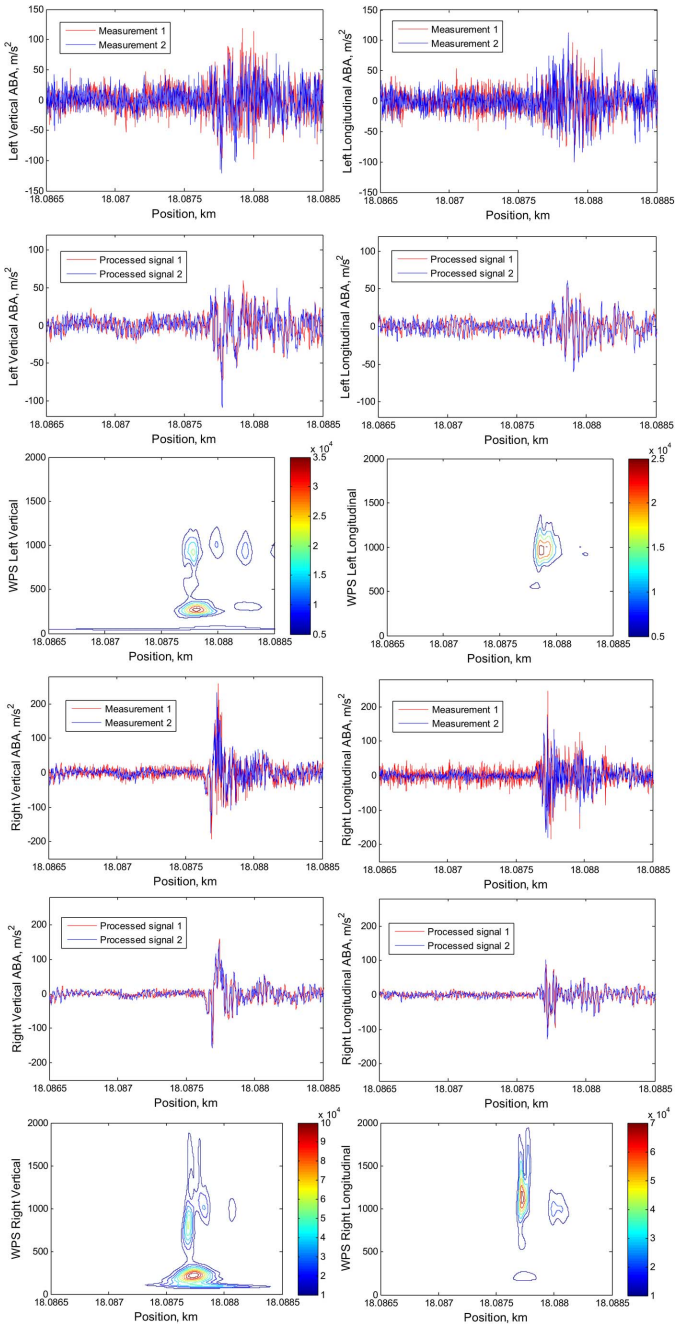

Fig. 13. Severe squat.

signal. For the signals of squat A (see Fig. 11), the WPS of the right longitudinal ABA signal is the strongest between 1000 and 2000 Hz (maximum magnitude 2.5 × 104). Thus, this defect is expected to be located in the right rail. There is also a peak in the right longitudinal signal. In the case of light squats, longitudinal ABA is more sensible and eases detection.

For comparison purposes, the ABA signals at squats B and C are also discussed. For both types of defects, the WPS of ABA in both the longitudinal and vertical directions can be used as an indicator for the presence of a defect. As expected, in the WPS, the maximum magnitudes are at lower frequencies than those for light squats, and the effects of the squats at ABA can be seen in both the vertical and longitudinal ABA signals. Multiple sensors reduce the likelihood of no hits due to hunting; thus, with this prototype and adequate data processing, the manual detection of moderate and severe squats reaches 100%. This concept has been verified on a large data set with eight measurement rounds between 2009 and 2011; each measurement round included three repetitive measurements on two sections of track with lengths of 3 km.

VII. Conclusion

In this paper, three improvements have been presented, including enhancement of ABA instrumentation and signal processing. The first improvement corresponds to the use of longitudinal ABA to enhance measurement sensitivity to light

squats, which are short-wave track irregularities. The second improvement considers the use of multiple sensors, noise-reduction techniques, and repeated measurements. The third improvement concerns the signal-processing solution for the reduction of disturbances from wheel defects. By using the improved instrumentation, the hit rate for moderate squats by manual data processing increased from 60% to 100%. By utilizing longitudinal ABA and application of noise-reduction techniques, the hit rate of small rail surface defects increased from 57% to 85%.

Because small rail surface defects include trivial defects, which are smaller than light squats, a higher hit rate may be achieved for light squats. These improvements enable the detection of squats at their earliest stage, when corrective maintenance actions can be taken. Utilization of this new measuring system and timely grinding can reduce the number of squats by 85% or more [42]. Those preliminary results were obtained by manual data processing.

Further research should extend the use of ABA for assessing health conditions of other railway assets, such as insulated joints, where misalignment of rail ends and bolt tightness are invisible to the naked eye and therefore cannot be judged by human inspectors. Other interesting applications could consider the analysis of wheelburns, corrugation, welds, switch frogs, and other track assets. The prototype will be further developed so that it can be installed on revenue trains to monitor networks at all times. This application will be particularly relevant for fast degradations for which the monitoring interval of six months, the most common practice with specialized measuring trains, is not sufficiently short.

Acknowledgment

The authors would like to thank the Associate Editor and anonymous reviewers for their valuable comments and suggestions.

References

[1] C. R. Sánchez, F. J. G. Fernández, L. C. Simón Vena, J. Carpio, and M. Castro, "Industrial telemaintenance: Remote management experience from subway to industrial electronics," *IEEE Trans. Ind. Electron.*, vol. 58, no. 3, pp. 1044–1051, Mar. 2011.

[2] M. P. Papaelias, C. Roberts, and C. L. Davis, "A review on non-destructive evaluation of rails: State-of-the-art and future development," in *Proc. Inst. Mech. Eng., Rail Rapid Transit*, 2008, vol. 222, pp. 367–384.

[3] J. Guzinski, H. Abu-Rub, M. Diguet, Z. Krzeminski, and A. Lewicki, "Speed and load torque observer application in high-speed train electric drive," *IEEE Trans. Ind. Electron.*, vol. 57, no. 2, pp. 565–574, Feb. 2010.

[4] N. Bosso, A. Gugliotta, and N. Zampieri, "A comprehensive strategy to estimate track condition and its evolution," *Int. J. Railway Technol.*, vol. 1, no. 2, pp. 1–19, 2012.

[5] S. D. Iwnicki and A. J. Bevan, "Damage to railway wheels and rails: A review of the causes, prediction methods, reduction and allocation of costs," *Int. J. Railway Technol.*, vol. 1, no. 1, pp. 121–146, 2012.

[6] H. Toliyat, K. Abbaszadeh, M. Rahimian, and L. E. Olson, "Rail defect diagnosis using wavelet packet decomposition," *IEEE Trans. Ind. Appl.*, vol. 39, no. 5, pp. 1454–1461, Sep./Oct. 2003.

[7] F. Marino, A. Distante, P. L. Mazzeo, and E. Stella, "A real-time visual inspection system for railway maintenance: Automatic hexagonal-headed bolts detection," *IEEE Trans. Syst. Man Cybern. C, Appl. Rev.*, vol. 37, no. 3, pp. 418–428, May 2007.

[8] M. P. Papaelias and M. Lugg, "Detection and evaluation of rail surface defects using alternating current field measurement techniques," in *Proc. Inst. Mech. Eng., Rail Rapid Transit*, 2012, vol. 226, pp. 530–541.

[9] Y. Li, H. Trinh, N. Haas, C. Otto, and S. Pankanti, "Rail component detection, optimization, assessment for automatic rail track inspection," *IEEE Trans. Intell. Transp. Syst.*, vol. 15, no. 2, pp. 760–770, Apr. 2014.

[10] B. Stratman, Y. Liu, and S. Mahadevan, "Structural health monitoring of railroad wheels using wheel impact load detectors," *J. Fail. Anal. Prev.*, vol. 7, no. 3, pp. 218–225, Jun. 2007.

[11] N. A. Thakkar, J. A. Steel, and R. L. Reuben, "Rail-wheel contact stress assessment using acoustic emission: A laboratory study of the effects of wheel flats," in *Proc. Inst. Mech. Eng., Rail Rapid Transit*, 2012, vol. 226, pp. 3–13.

[12] M. J. S Lowe and P. Cawley, Long Range Guided Wave Inspection Usage—Current Commercial Capabilities and Research Directions, (accessed 2014). [Online]. Available: http://www3.imperial.ac.uk/nde/publications

[13] C. Esveld, *Modern Railway Track*, 2nd ed. Zaltbommel, The Netherlands, MRT-Productions, 2001. [Online]. Available: http://www.esveld.com/MRT.html

[14] J. S. Wang and C. Fang-Chen, "An accelerometer-based digital pen with a trajectory recognition algorithm for handwritten digit and gesture recognition," *IEEE Trans. Ind. Electron.*, vol. 59, no. 7, pp. 2998–3007, Jul. 2012.

[15] Z. Wen-Hong and T. Lamarche, "Velocity estimation by using position and acceleration sensors," *IEEE Trans. Ind. Electron.*, vol. 54, no. 5, pp. 2706–2715, Oct. 2007.

[16] O. Vainio, "Adaptive derivative estimation for delay-constrained acceleration measurement," *IEEE Trans. Ind. Electron.*, vol. 46, no. 5, pp. 933–935, Oct. 1999.

[17] J. S. Lee, S. Choi, S. S. Kim, C. Park, and Y. G. Kim, "A mixed filtering approach for track condition monitoring using accelerometers on the axle box and bogie," *IEEE Trans. Instrum. Meas.*, vol. 61, no. 3, pp. 749–758, Mar. 2012.

[18] G. M. Shafiullah, S. A. Azad, and A. B. M. Shawkat Ali, "Energy-efficient wireless MAC protocols for railway monitoring applications," *IEEE Trans. Intell. Transp. Syst.*, vol. 14, no. 2, pp. 649–659, Jun. 2013.

[19] Y. Sunaga, I. Sano, and T. Ide, "A practical use of axlebox acceleration to control the short wave track irregularities," Railway Tech. Res. Inst. Quarterly Rep., vol. 38, no. 4, 1997.

[20] A. Massel, "Power spectrum analysis—Modern tool in the study of rail surface corrugations," *NDT & E Int.*, vol. 32, no. 8, pp. 429–436, Dec. 1999.

[21] M. Bocciolone, A. Caprioli, A. Cigada, and A. Collina, "A measurement system for quick rail inspection and effective track maintenance strategy," *Mech. Syst. Signal Proc.*, vol. 21, no. 3, pp. 1242–1254, Apr. 2007.

[22] A. Caprioli, A. Cigada, and D. Raveglia, "Rail inspection in track maintenance: A benchmark between the wavelet approach and the more conventional Fourier analysis," *Mech. Syst. Signal Proc.*, vol. 21, no. 2, pp. 631–652, Feb. 2007.

[23] H. Tanaka and A. Furukawa, "The estimation method of wheel load and lateral force using the axlebox acceleration," in *Proc. 8th World Congr. Railway Res.*, 2008, pp. 1–10.

[24] Z. Li and M. Molodova, "Method and instrumentation for detection of rail defects," in Particular Rail top Defects, Eur. Patent, WO2011019273 (A1)-2011-02-17, 2011.

[25] M. Molodova, Z. Li, and R. Dollevoet, "Axle box acceleration: Measurement and simulation for detection of short track defects," *Wear*, vol. 271, no. 1/2, pp. 349–356, May 2011.

[26] M. Molodova, Z. Li, A. Núñez, and R. Dollevoet, "Automatic detection of squats in the railway infrastructures," *IEEE Trans. Intell. Transp. Syst.*, vol. 15, no. 5, pp. 1980–1990, Feb. 2014.

[27] O. F. Eker *et al.*, "A simple state-based prognostic model for railway turnout systems," *IEEE Trans. Ind. Electron.*, vol. 58, no. 5, pp. 1718–1726, May 2011.

[28] A. Soualhi, H. Razik, G. Clerc, and D. D. Doan, "Prognosis of bearing failures using hidden Markov models and the adaptive neuro-fuzzy inference system," *IEEE Trans. Ind. Electron.*, vol. 61, no. 6, pp. 2864–2874, Jun. 2014.

[29] X. Jin, M. Zhao, T. Chow, and M. Pecht, "Motor bearing fault diagnosis using trace ratio linear discriminant analysis," *IEEE Trans. Ind. Electron.*, vol. 61, no. 5, pp. 2441–2451, May 2014.

[30] L. He, J. Xiong, H. Ouyang, P. Zhang, and K. Zhang, "High-performance indirect current control scheme for railway traction four-quadrant converters," *IEEE Trans. Ind. Electron.*, vol. 61, no. 12, pp. 6645–6654, Dec. 2014.

[31] M. A. Hassan, A. M. E. Bayoumi, and Y. J. Shin, "Quadratic nonlinearity index based on bicoherence and its application in condition monitoring of drive-train components," *IEEE Trans. Instrum. Meas.*, vol. 63, no. 3, pp. 719–728, Mar. 2014.

[32] H. Feng *et al.*, "Automatic fastener classification and defect detection in vision-based railway inspection systems," *IEEE Trans. Instrum. Meas.*, vol. 63, no. 4, pp. 877–888, Apr. 2014.
[33] A. V. Ovanesova and L. E. Suárez, "Applications of wavelet transforms to damage detection in frame structures," *Eng. Struct.*, vol. 26, no. 1, pp. 39–49, Jan. 2004.
[34] I. Daubechies, "The wavelet transform, time–frequency localization and signal analysis," *IEEE Trans. Inf. Theory*, vol. 36, no. 5, pp. 961–1005, Sep. 1990.
[35] Bruel and Kjaer, Structural Testing: Mechanical Mobility Measurements, (accessed 2014). [Online]. Available: http://www.bksv.com/library/primers
[36] D. J. Thompson, "Theoretical modelling of wheel–rail noise generation," *Proc. Inst. Mech. Eng., Rail Rapid Transit*, vol. 205, no. 2, pp. 137–149, 1991.
[37] F. J. Periard, "Wheel–Rail Noise Generation: Curve Squealing by Trams," Ph.D. dissertation, TU Delft, Delft, The Netherlands, 1998.
[38] Bruel and Kjaer, Handbook of Piezoelectric Accelerometers, (accessed 2014). [Online]. Available: www.bksv.com/doc/bb0694.pdf
[39] O. Rompelman and H. H. Ros, "Coherent averaging technique: A tutorial review. Part 1: Noise reduction and the equivalent filter," *J. Biomed. Eng.*, vol. 8, no. 1, pp. 24–29, Jan. 1986.
[40] S. Beskhyroun, T. Oshima, and S. Mikami, "Wavelet-based technique for structural damage detection," *Struct. Control Health Monit.*, vol. 17, no. 5, pp. 473–494, Aug. 2010.
[41] P. Terwiesch, S. Menth, and S. Schmidt, "Analysis of transients in electrical railway networks using wavelets," *IEEE Trans. Ind. Electron.*, vol. 45, no. 6, pp. 955–959, Dec. 1998.
[42] A. Zoeteman, R. Dollevoet, and Z. Li, "Dutch research results in Wheel Rail Interface Management: 2001–2013 and beyond," *Proc. Inst. Mech. Eng., Rail Rapid Transit*, vol. 228, no. 6, pp. 642–651.

Zili Li received the B.Sc. and M.Sc. degrees in mechanical engineering from Southwest Jiaotong University, Chengdu, China, in 1988 and 1991, respectively, and the Ph.D. degree from Delft University of Technology, Delft, The Netherlands, in 2002.

Between 1999 and 2005, he was with the Institute of Road Transportation of TNO, Delft, where he was engaged in research and software development of multibody dynamics and finite-element method for crash safety. In 2005, he joined the Faculty of Civil Engineering and GeoSciences, Delft University of Technology, where he taught and performed research on railway engineering. He is currently an Associate Professor with the Section of Road and Railway Engineering, Delft University of Technology. His research interests include numerical solution of frictional rolling contact and its applications to analyses of wear, rolling contact fatigue, and vehicle dynamics; train–track interaction, particularly in the high-frequency/short-wave range and at switches and crossings; condition monitoring of tracks; and friction adhesion between wheel and rail.

Maria Molodova received the M.Sc. degree in mechanical engineering from N. I. Lobachevsky State University of Nizhny Novgorod, Nizhni Novgorod, Russia, in 2005, with a thesis on numerical modeling of the electrohydroimpulsive stamping process, and the Ph.D. degree from Delft University of Technology, Delft, The Netherlands, in 2013, with a thesis on the development of detection algorithms for tracking short-wave defects and their causes in the wheel–track system by means of axle box acceleration measurements.

She is currently with the Section of Road and Railway Engineering, Delft University of Technology. Her research interests include the implementation of coupled implicit–explicit finite-element methods for time-domain simulations of wheel–track systems and signal processing techniques for frequency-domain investigation of simulated and real-life measured data.

Alfredo Núñez (M'02–SM'14) received the Ph.D. degree in electrical engineering from the Universidad de Chile, Santiago, Chile, in 2010.

He was a Postdoctoral Researcher with the Delft Center for Systems and Control. He is currently with the Section of Road and Railway Engineering, Delft University of Technology, Delft, The Netherlands. He authored the book *Hybrid Predictive Control for Dynamic Transport Problems* in the Series of Advances in Industrial Control (Springer-Verlag, 2013). His research interests include monitoring and maintenance of railway infrastructure, modeling and control of traffic and transportation systems, model predictive control, and fuzzy systems.

Rolf Dollevoet received the M.Sc. degree in mechanical engineering from Eindhoven University of Technology, Eindhoven, The Netherlands, and the Ph.D. degree from the University of Twente, Enschede, The Netherlands, in 2010.

Since 2003, he has been with ProRail, Utrecht, The Netherlands. Since 2012, he has been appointed as a part-time Professor with the Section of Road and Railway Engineering, Delft University of Technology, Delft, The Netherlands. He is also currently the leader of scientific research on rolling contact fatigue and wheel–rail interface within ProRail Civil Engineering and the Chair of the International Union of Railways working group on wheel–rail conditioning and lubrication.

Dr. Dollevoet was a recipient of the Jan van Stappen Spoorprijs 2010 Award (a yearly prize for contributions to the travel quality and service for passengers in The Netherlands) from the railway sector for his Ph.D. research and its huge potential to reduce track maintenance costs.